The gradient wind in the mesosphere and lower thermosphere

Ruth S. Lieberman

Colorado Research Associates, 3380 Mitchell Lane, Boulder, CO 80301, U.S.A.

HRDI zonally averaged daytime temperatures are used to compute the gradient wind in the 65–105 km range. Results are compared with independently measured HRDI zonal mean zonal winds. The gradient wind captures the essential features of the observed wind field in the summertime midlatitudes, including the stratospheric easterly (westward) jet and the reversal to westerly (eastward) winds in the lower thermosphere. The consistency between HRDI and gradient winds diminishes at tropical latitudes, due to substantial tidal contamination of daytime temperatures used to compute the gradient wind.

1. Introduction

Zonally averaged zonal winds and temperatures in the middle atmosphere are commonly assumed to be in thermal wind balance (Andrews *et al.*, 1987; Fleming *et al.*, 1990; Hedin *et al.*, 1996). The gradient wind approximation has been shown by Randel (1987) to be generally quite accurate in the stratosphere. Manson *et al.* (1991) compared medium frequency (MF) radar winds in the 60–120 km range with gradient winds computed from the COSPAR International Reference Atmosphere 1986 temperature database, hereafter referred to as CIRA-86. Good agreement between the two sets of winds was reported below 80 km; however, above this level radar winds deviated systematically from CIRA-86 gradient winds. In particular, the gradient wind approximation produced jet maxima that are stronger than observed, and placed the level of the wind reversal too high. Fleming *et al.* (1996) compared CIRA-86 gradient winds to winds directly observed by the high resolution Doppler Imager (HRDI) and the wind imaging interferometer (WINDII) on board the Upper Atmosphere Research Satellite (*UARS*). In the lower mesosphere HRDI and CIRA-86 wind climatologies showed good agreement in reproducing the general structural and seasonally-varying features of the midlatitude circulation. Differences between CIRA-86 and *UARS* winds were more pronounced above the mesopause. These were attributed by the authors to differences in spatial coverage and vertical resolution, and possible ageostrophic influences.

HRDI recovers daytime temperatures along with horizontal winds in the 65–105 km range. The availability of these two independently measured fields allows for a quantitative assessment of the gradient wind approximation. Unlike the mid-upper troposphere and stratosphere which are largely inviscid, the mesosphere and lower thermosphere (MLT) are regions of strong-amplitude wave breakdown and turbulence production. These processes act as a drag upon the large-scale flow, and thus can destroy geostrophic (or gradient)

wind balance. It is of interest to examine the validity of the gradient wind approximation in a region of the atmosphere which is inherently ageostrophic.

This paper reports a comparison between MLT zonal mean winds directly observed by HRDI, and gradient zonal mean winds computed from HRDI temperatures. It must be emphasized that the use of daytime-only winds and temperatures in this context requires careful consideration of tidal effects. Diurnal tides, which are highly ageostrophic motions, cannot be fully separated from the long-term (i.e., climatological) component of HRDI zonally averaged winds and temperatures (Hays *et al.*, 1994; Ortland *et al.*, 1998). Consequently, this study focuses on two solstice periods, 11 December 1993–9 February 1994, and 13 June–12 August 1994, that are characterized by strong extratropical mean circulations and weak diurnal amplitudes (Burrage *et al.*, 1995; Lieberman, 1997). Thermal wind balance at the equator is also examined, using a composite year of HRDI winds and temperatures.

The following section describes the HRDI data, and mean wind and temperature analyses. Section 3 presents the geostrophic and gradient wind fields, and their comparisons with HRDI winds. Discussion of the results and an appraisal of possible tidal effects appear in Section 4. Section 5 summarizes the findings, and discusses future observational requirements.

2. HRDI Data and Analysis

HRDI is a Fabry-Perot interferometer/photometer designed to measure stratospheric and MLT horizontal winds, and MLT temperatures. MLT winds are inferred from the Doppler shift of O_2 atmospheric band emission features. Temperatures are determined along with volume emission rates by considering perturbations of two O_2 lines about a reference brightness calculation. Daytime MLT winds are recovered between 60–110 km with a precision of about $5\,\mathrm{m\,s^{-1}}$ (Burrage *et al.*, 1996b). Daytime temperatures are retrieved between 65 and 105 km, with an error of 7K (Ortland *et al.*, 1998). Nighttime winds about the 95 km level are deter-

mined from O_2 band emissions in a thin layer between 90 and 95 km (Burrage et al., 1994). HRDI design, operation, and data retrieval procedures are discussed extensively by Abreu et al. (1989), Hays et al. (1993), and Ortland et al. (1995, 1998); the interested reader is referred to these papers for further details.

HRDI commenced routine viewing of the MLT in November 1991. Between January 1992 and April 1994 HRDI nominally sampled the daytime mesosphere on alternating days, while between April 1994 and 1995 HRDI sampled the mesosphere almost daily, but on alternate orbits. Nighttime winds near 95 km were sampled daily between October 1992 and April 1995. Since the failure of the *UARS* solar array drive in April 1995, HRDI measurements have been carried out with diminishing frequency and continuity; as a result only measurements between 1992–April 1995 are included in the analyses.

The present study uses version 11 of HRDI level 2 winds and temperatures, archived at the University of Michigan Space Physics Research Laboratory. (A gridded, interpolated, "level 3A" version of these data is archived and distributed by Goddard Space Flight Center.) Daytime MLT winds and temperatures are collected for each day in latitude bins 5 degrees wide, and then averaged in longitude. This procedure is intended to highlight the zonal mean component; however, because HRDI daytime measurements are nominally made at nearly the same local time on an individual day, it should be borne in mind that the longitudinal average highlights the migrating (i.e., local-time dependent) diurnal and semidiurnal tides (Morton et al., 1993; Hays et al., 1994). The precession of the *UARS* orbit results in a 20 minute day-to-day drift in the local time sampling. Approximately 12 daytime hours are sampled over one complete yaw cycle (36 days) under equinoctial conditions.

Two solstice-centered intervals are considered, 11 December 1993–9 February 1994 and 13 June–12 August 1994. These periods are chosen because of the strong extratropical zonal mean circulation in the MLT. Moreover, the amplitude of the (1,1) diurnal tide during these periods is weaker by a factor of 2 than the preceding and following years (Burrage et al., 1995; Lieberman, 1997), Thus, tidal aliasing of the zonal mean winds and temperatures is relatively minimal (although by no means negligible; see Section 4). The length of the analysis period, 60 days, is chosen in order to maximize HRDI local time sampling during solstice conditions in both hemispheres.

Figure 1 illustrates the local time coverage as a function of latitude during 11 December 1993–9 February 1994 and 13 June–12 August 1994. For each of these intervals, daily longitudinal averages of zonal wind and temperature are formed, sorted into 12 local time bins (observations between 1200 and 2300 LT are binned with those between 0000 and 1100 LT), and then averaged. If data at a given latitude span at least 10 hours, and are missing over no more than 4 consecutive local time bins, an average over all filled local time bins is then performed. This procedure maximizes latitude coverage of the seasonal (or 60-day) mean, while minimizing local time sampling biases and contamination by the semidiurnal tides. (Note, however, that the effects of diurnal tides cannot be fully removed.)
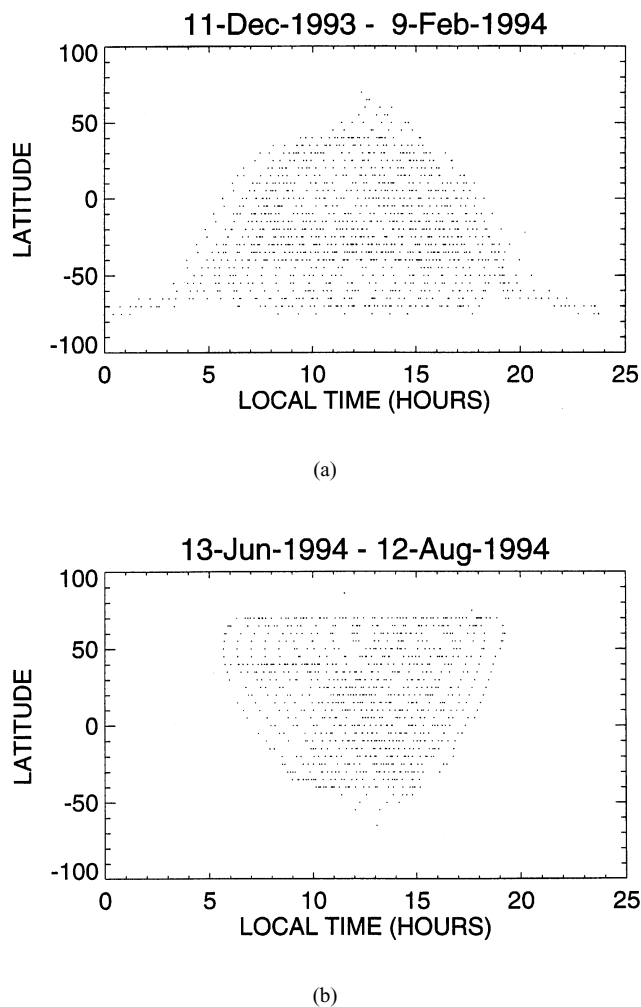

(a)

(b)

Fig. 1. Local time coverage vs. latitude during 11 December 1993–9 February 1994 (a) and 13 June–12 August 1994 (b).

Figure 2 shows HRDI zonal mean temperatures averaged about the December and July solstices. As mentioned previously, data are plotted only at latitudes with sufficient coverage spanning 10 hours between 0000 and 1200 LT. During both solstice periods, the high latitude summer MLT is dominated by a broad deep cold region, with a temperature minimum of 145K centered at 90 km. The midlatitude summer MLT is characterized during both periods by strong meridional temperature gradients between 75 and 90 km. During December 1993–February 1994, a shallow inversion layer is present between 80 and 85 km from 25°S–40°N, evidenced by the looping of the 200K contour. Vertical temperature profiles between the equator and 30°N (not shown) indicate that the temperature excursion in the inversion layer is about 7K. Similar inversion structures have been reported in Rayleigh and Na lidar temperatures at Northern hemisphere midlatitudes (She et al., 1995; Leblanc and Hauchecorne, 1997). The inversion is also present in the Southern hemisphere winter (13 June–12 August 1994), but is contained between 30°S and 10°S. Above 85 km temperatures again decrease throughout the tropics and midlatitudes, reaching a minimum at about 95 km. During 11 December 1993–9 February 1994, the equatorial minimum in HRDI temperatures is several de-
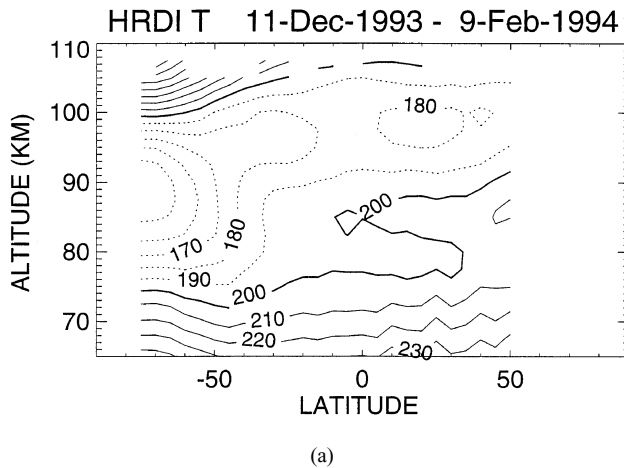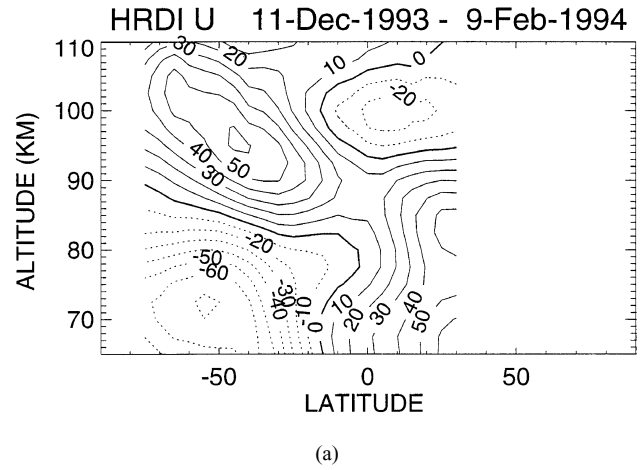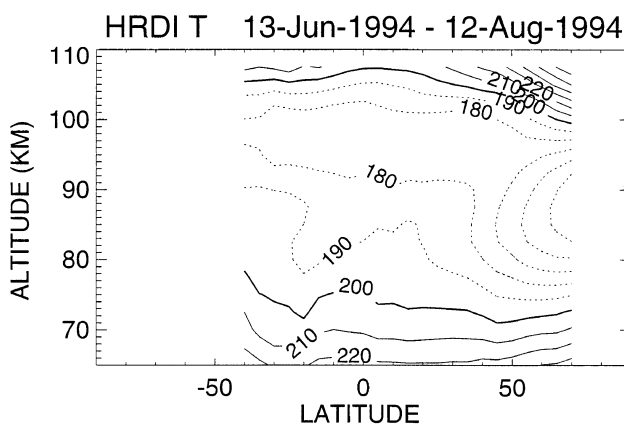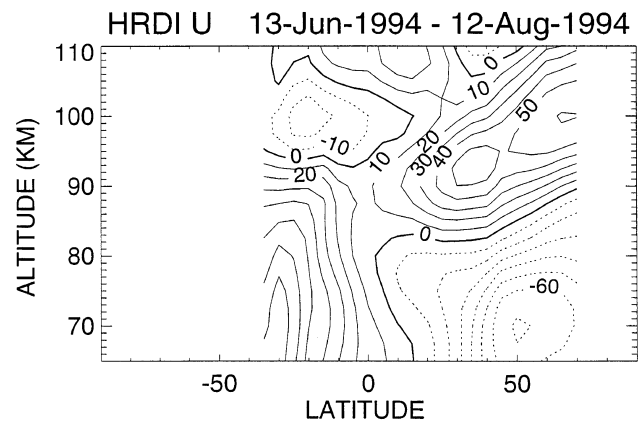
Fig. 2. HRDI zonal mean temperatures. Contour interval is 10K. Dotted contours enclose temperatures colder than 200K. (a) 11 December 1993–9 February 1994. (b) 13 June–12 August 1994.

Fig. 3. HRDI zonal mean zonal winds. Contour interval is $10\,\mathrm{m\,s^{-1}}$. Dotted contours represent negative values, or easterly flow. (a) 11 December 1993–9 February 1994. (b) 13 June–12 August 1994.

grees warmer than in the neighboring extratropical latitudes.

HRDI solstice zonal mean winds are plotted in Fig. 3, binned and averaged identically to the temperature field. The summer hemisphere is characterized by easterly flow which peaks near 75 km, with a transition to westerly winds occurring between 80 and 90 km along an axis tilting upward and poleward. The winter hemisphere is characterized by a deep layer of westerlies, which reversing to easterlies at 95 km.

Figure 4(a) shows composite monthly averages of HRDI equatorial zonal mean winds, formed from observations between January 1992 and April 1995. The dominant feature in the wind field is the well-documented mesopause semiannual oscillation, or MSAO (Lieberman *et al.*, 1993; Burrage *et al.*, 1996a; Garcia *et al.*, 1997) below 90 km. Strong easterly winds occur at equinox, separated by weak westerly winds at solstice (see Fig. 3). Above 90 easterly winds prevail, with a weak semiannual signal juxtaposed. This flow pattern has been linked by Lieberman and Hays (1994) and Lieberman (1997) to the presence of diurnal zonal winds, and to momentum deposition by dissipating diurnal tides.

Figure 4(b) shows the composite monthly mean temperature as a perturbation from the time-mean (January 1992–

April 1995) field. The dominant variability here is also semiannual. The highest perturbation values are centered near 90 km, with maxima at equinox and minima at solstices. This seasonal behavior may be related to aliasing of daytime temperatures by the diurnal tides, as discussed further in Section 4. Below 90 km, temperature perturbations are weaker by a factor of two, but exhibit a clear semiannual variation that is $180°$ out of phase with the oscillation above 90 km. Perturbation maxima appear during solstices, separated by minima at equinox, and move downward in time. This behavior is consistent with the MSAO documented in Solar Mesospheric Explorer (SME) temperatures (Garcia and Clancy, 1990; Garcia *et al.*, 1997), although the HRDI MSAO is slightly weaker.

3.   Gradient and Geostrophic Winds
3.1   Midlatitude calculations

The gradient zonal mean wind is calculated from the leading terms of the zonally averaged meridional momentum equation. Assuming steady state conditions, and neglecting eddy fluxes and advection by the mean meridional circula-

COMPOSITE WIND

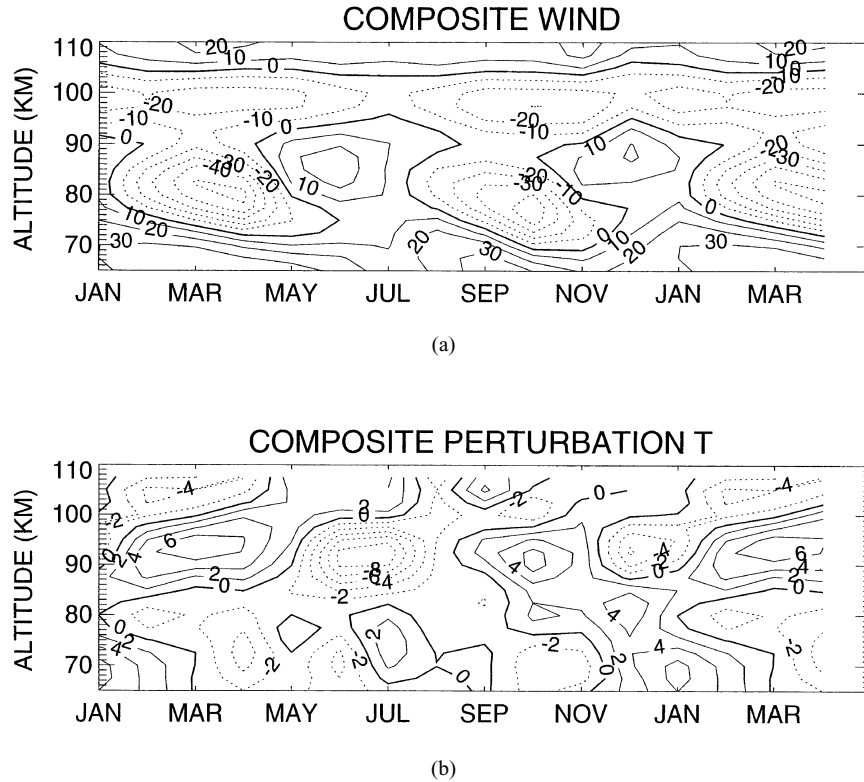(a)

COMPOSITE PERTURBATION T

(b)

Fig. 4. (a) Composite monthly mean HRDI zonal mean winds. (b) Composite monthly mean zonal mean temperature, with the time average removed. The first 4 months of the year are repeated on the abscissa.

tion, the remaining terms are

$$\overline{U}\left(f + \frac{\overline{U}\tan\phi}{a}\right) = -\frac{\overline{\Phi}_\phi}{a} \tag{1}$$

(Andrews *et al.*, 1987). Following Hitchman and Leovy (1986), the zonal mean wind inside the parenthesis is approximated as the geostrophic wind

$$\overline{U}_g = -\frac{\overline{\Phi}_\phi}{fa}. \tag{2}$$

Gradient winds are traditionally computed by applying (1) and (2) to temperature data and "tie-on" geopotential heights (Hitchman and Leovy, 1986; Randel, 1987). Unfortunately, the lower boundary of HRDI temperature retrievals is at 65 km, well above the highest level (about 50 km) at which daily geopotential analyses are provided by the National Center for Environmental Prediction (NCEP) and the United Kingdom Meteorological Office (UKMO) operational weather prediction models. An alternative formulation is obtained by differentiating (1) with respect to the scaled log-pressure coordinate *z*, and applying the hydrostatic relation

$$\overline{\Phi}_z = H^{-1}R\overline{T} \tag{3}$$

to obtain

$$\frac{\partial \overline{U}}{\partial z} + p(z)\overline{U} = q(z) \tag{4}$$

where

$$p(z) = \frac{\partial \overline{U}_g}{\partial z}(2a\Omega\cos\phi + \overline{U}_g)^{-1} \tag{5}$$

and

$$q(z) = \frac{-R\overline{T}_\phi}{H(af + \overline{U}_g\tan\phi)}. \tag{6}$$

Equation (4) is a first-order differential equation which can be readily solved given an appropriate boundary condition for $\overline{U}$. Fleming *et al.* (1996) have shown that away from the tropics, UARS seasonally averaged zonal mean zonal winds agree well with CIRA-86 gradient winds at 66 km. Thus, $\overline{U}$ is set to the HRDI wind at 65 km, and (4)–(6) are solved entirely from HRDI observations. The vertical shear of the geostrophic wind, required to evaluate $p(z)$, is determined from HRDI zonal mean temperatures according to

$$\frac{\partial \overline{U}_g}{\partial z} = \frac{-R}{Hfa}\overline{T}_\phi. \tag{7}$$

The geostrophic wind U_g, required to evaluate $q(z)$, is found by integrating (7) with respect to z. Using Eq. (1) with the condition that $\overline{U} = \overline{U}_{HRDI}$ at 65 km gives the following boundary value for $\overline{U}_g$ at 65 km:

$$\overline{U}_g = \overline{U}_{HRDI}\left(1 - \frac{\overline{U}_{HRDI}}{2a\Omega\cos\phi}\right)^{-1}. \tag{8}$$

Given the coefficients $p(z)$ and $q(z)$ and the lower boundary condition, (4) is then solved for $\overline{U}$ by the method of variation of parameters.

Gradient wind calculations are presented in Fig. 5. Comparison with observed HRDI winds (Fig. 3) shows that the
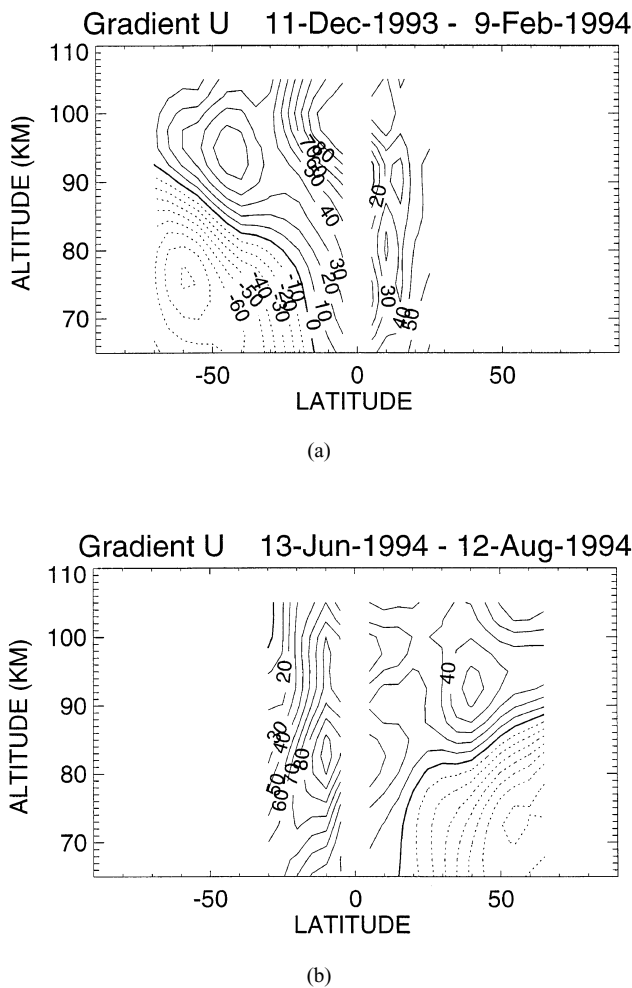
(a)

(b)

Fig. 5. Gradient zonal mean wind computed from temperatures in Fig. 2. (a) 11 December 1993–9 February 1994. (b) 13 June–12 August 1994. Values are smoothed with a 3-point running mean in latitude.

gradient approximation reproduces the essential features of the midlatitude winds in the summer hemisphere. These include the closure of the easterly jet near 75 km, the reversal to westerly flow between 85 and 95 km, and a westerly wind maximum near 95 km. For the December 1993–February 1994 interlude, gradient easterly wind maxima are slightly stronger than observed winds, while gradient westerly winds are slightly weaker. In the northern hemisphere summer (June–August 1994), the gradient wind approximation captures an easterly maximum near 75 km, and a westerly maximum near 45°N. An additional westerly wind peak of 60 m s^{-1} observed at 65°N does not appear in the gradient wind field.

The consistency between the gradient and HRDI summer winds deteriorates equatorward of 30 degrees. The gradient zero wind line in the summer hemisphere does not extend as far equatorward as the observed zero winds. As a result, gradient winds in the tropical summer latitudes are westerly between 65 and 85 km, while observed wind are easterly. Similarly, the gradient wind fails to reproduce the intrusion of winter hemisphere lower thermospheric easterlies across the equator, resulting in an excess of gradient westerly winds

above 95 km. While HRDI and gradient tropical winds are both directed westerly between 85 and 95 km, the gradient approximation greatly overestimates the westerly winds in this region.

3.2 Geostrophic balance at the equator

Equatorial zonally averaged winds and temperatures have been shown to obey thermal wind balance in the stratosphere (Andrews et al., 1987; Fleming and Chandra, 1989). The assumption of thermal wind balance in the equatorial MLT has been invoked to deduce MSAO zonal winds from temperatures (Garcia and Clancy, 1990) and conversely, to infer MSAO temperatures from zonal winds (Palo and Avery, 1993). More recently, Garcia et al. (1997) compared the HRDI vertical wind shears at the equator with the vertical shear of the geostrophic wind derived from SME temperatures. The two fields compared well qualitatively below 80 km, but differed in magnitude and sign above this level, possibly because of tidal contamination of SME temperatures.

The present study enables an examination of geostrophy at the equator using simultaneous HRDI wind and temperature measurements. Latitude-height projections of composite time-mean and monthly averaged HRDI MLT temperature (not shown) indicate that the meridional gradient of the zonal mean temperature is quite weak at the equator. Thus, following Fleming and Chandra (1989), L'Hopitals' rule is invoked and Eq. (1) is differentiated with respect to latitude, and evaluated at the equator to yield

$$\frac{\overline{U}^2}{a} + 2\Omega\overline{U} = -\frac{\overline{\Phi}_{\phi\phi}}{a}. \tag{9}$$

Neglecting the first term on the LHS of (9) and differentiating the remaining terms with respect to z yields

$$\overline{U}_z = -\frac{R}{2a\Omega H}\overline{T}_{\phi\phi}. \tag{10}$$

The RHS and LHS terms in Eq. (10) are calculated from equatorial values of perturbation $\overline{T}$ and $\overline{U}$ (shown in Fig. 4), and plotted in Fig. 6. The wind shear is fully dominated by the MSAO. The variation of the temperature curvature [RHS of (10)] is also predominantly semiannual; however the vertical structure is more complicated than that of the wind shear. Below 90 km the two fields show good general phase agreement, with downward descent in time. The negative (or easterly) phase of the MSAO wind shear descends from 80 km to 65 km between January and June. A similar pattern is embedded in the temperature curvature field, punctuated by a locally strong positive curvature in May. The transition to positive MSAO-related curvature occurs in conjunction with the westerly wind shear (in June) between 75 and 85 km. Unlike the wind shear, however, negative temperature curvature persists below 70 km until September. The "second" easterly phase of the wind shear starts descending from the 80 km level in August, reaching 65 km by November. The corresponding transition in the temperature field is not as fully realized, where only very weakly negative curvatures prevail. Above 90 km the temperature curvature term is much stronger than the vertical wind shear, and exhibits additional structure above 100 km that is absent altogether from the wind shear field. This behavior may be due to strong tidal influences, as discussed in the following section.
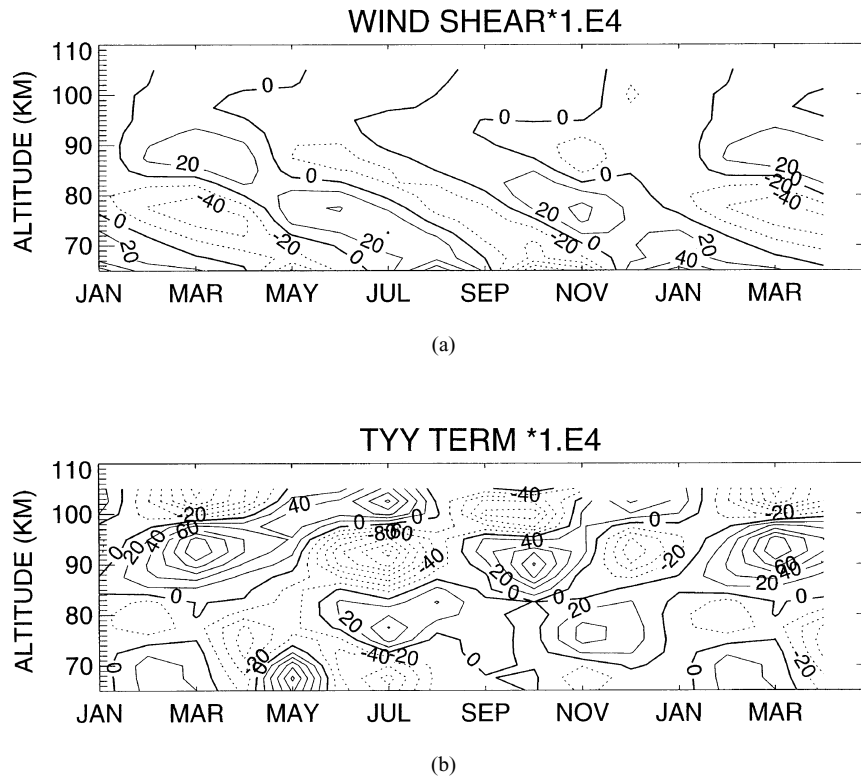
Fig. 6.   Composite monthly mean (a) vertical shear of perturbation HRDI equatorial zonal mean wind. (b) RHS of Eq. (10), using HRDI perturbation temperatures shown in Fig. 4(b). Units are s^{-1}. Fields are scaled by 10^4.

4.   Discussion

HRDI daytime zonal mean winds and temperatures are examined for gradient wind balance at middle and high latitudes in the summer hemisphere. The gradient wind field reproduces the basic observed midlatitude summer structure: the mesospheric easterly jet, and the transition to a westerly lower thermospheric jet. This MLT circulation has been shown to result from zonal momentum deposition by breaking gravity waves (Leovy, 1964; Andrews *et al.*, 1987).

Although visual inspection of Figs. 3 and 5 suggests a high level of consistency between HRDI and gradient winds at extratropical summer latitudes, quantitative consideration of the terms in Eq. (1) shows that strong ageostrophic zonal mean winds do exist. Figure 7 shows the difference between the LHS and the RHS of Eq. (1), which would vanish if HRDI winds and temperatures obeyed gradient wind balance everywhere. As before, the term inside the parenthesis is approximated by $\overline{U}_g$. HRDI winds are substituted for $\overline{U}$ appearing outside the parenthesis on the LHS of (1), and (2) is used to evaluate the RHS of (1).

Strong meridional accelerations are seen at the high summer latitudes. Large values are found near the HRDI zero wind line during December solstice, and within the westerly jet during both solstices above 100 km. Typical extratropical momentum residuals are on the order of 300–400 m s^{-1}day^{-1}, with peak values of 500 m s^{-1}day^{-1} in the westerly jets. To some extent, these values reflect the propagation of HRDI temperature uncertainties into the wind calculation. Equation (7), when applied at 45°S with meridional and ver-

tical increments of 5° and 2.5 km respectively, shows that a 7K uncertainty in the latitudinal temperature difference implies a maximum uncertainty of about 13 m s^{-1} in $\overline{U}_g$, or a momentum residual of about 112 m s^{-1}day^{-1}. While this error is significant, it does not account for the full range of meridional momentum residuals in Fig. 7. Physical causes of meridional wind accelerations include momentum advection by the mean meridional circulation, and momentum deposition in the north-south direction by gravity waves (Andrews *et al.*, 1987). Schoeberl *et al.* (1983) estimated the drag associated with meridional propagation of gravity waves, and found it to be on the order of the zonal drag for horizontally isotropic waves. Typical values cited for MLT gravity-wave drag in the zonal direction are usually near 100 m s^{-1}day^{-1} (Andrews *et al.*, 1987; Huang and Smith, 1991), or about 1/3–1/4 of the highest numbers shown in Fig. 7.

Residual meridional accelerations are also seen above 90 km equatorward of 30°. These may also reflect temperature error propagation, which become more severe at latitudes due to the presence of the Coriolis term in the denominators of the RHS sides of Eqs. (2) and (3). However, MLT diurnal tides have substantial amplitudes at these latitudes (Hays *et al.*, 1994; McLandress *et al.*, 1996; Khattatov *et al.*, 1997). As mentioned previously, these motions cannot be fully filtered from the averaged daytime wind and temperature fields. This limitation is illustrated clearly in Fig. 8, which shows daytime HRDI meridional winds averaged in the same manner used to produce the zonal wind and temperature fields in Figs. 2 and 3, respectively. The low latitudes
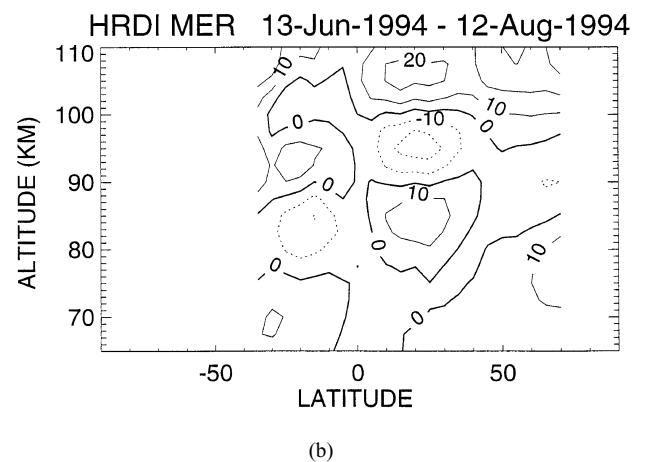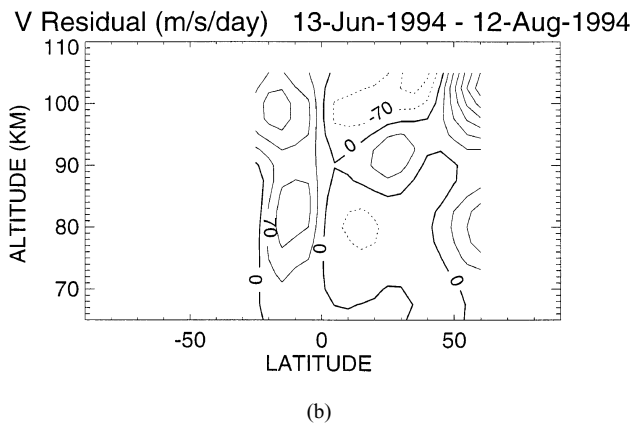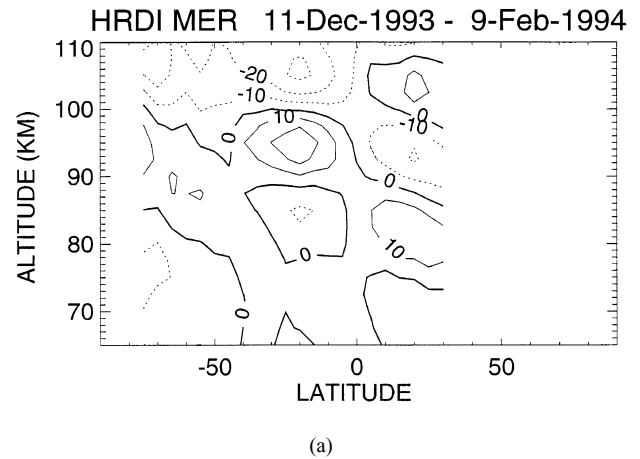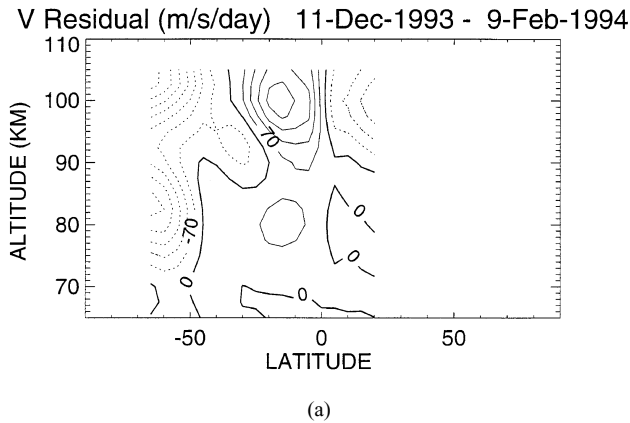
Fig. 7. Residual meridional acceleration, in m s^{-1}day^{-1}. (a) 11 December 1993–9 February 1994. (b) 13 June–12 August 1994. Values are smoothed using a 3-point running mean in latitude.

Fig. 8. As in Fig. 3, for meridional winds. (a) 11 December 1993–9 February 1994. (b) 13 June–12 August 1994.

are dominated by the effects of the partially filtered diurnal tide. The morphology of the (1,1) mode is clearly visible as alternating layers of northward and southward winds that exhibit asymmetry about the equator.

Diurnal temperatures and zonal winds are on the order of climatological (or time-mean) variability, and are therefore not as readily discernible in the daytime average fields (Figs. 2 and 3), nor can they be extracted by means of harmonic or modal fits (Hays *et al.*, 1994; Lieberman and Hays, 1994; Forbes *et al.*, 1997). Information about the diurnal tide can nonetheless be obtained by examining the spatial structure of differences between measurements taken close to 12 hours apart. Such a difference field minimizes the time-mean and the 12-hour harmonic, while enhancing the diurnal tide at a particular phase. For a propagating diurnal tide, a fixed local time "snapshot" can provide information about the amplitude and the dominant zonal and vertical wavenumber. This strategy was employed by Wallace and Hartranft (1969) and Wallace and Tadd (1974) to examine diurnal tides in rawindsone data, and by Hitchman and Leovy (1985) and Lieberman (1991) to describe the propagating diurnal tide in the stratosphere.

For the solstice periods under consideration, maximum latitude coverage by HRDI is obtained with an 11-hour dif-

ference field, formed from observations at 1700 and 0600 LT. Temperature differences obtained in this manner (and divided by 2) are plotted in Fig. 9. A prominent warm perturbation is centered over the equator between 85 and 95 km, with a magnitude of about 15K. The perturbation reverses sign near 100 km and rapidly attenuates above that level. Below 85 km the difference field shows a strong cold perturbation whose maximum is shifted toward the winter hemisphere. The confinement of the strong 12-hour differences to the equatorial latitudes, and the reversing of the sign every 10 km in the vertical is qualitatively consistent with the behavior of the diurnal tide (Chapman and Lindzen, 1970; Forbes, 1982; Yudin *et al.*, 1997). The 11-hour temperature difference field below 85 km suggests a 25K perturbation minimum, and a vertical half-wave length well in excess of 15 km. This behavior is much less consistent with tidal theory, and may reflect the temporal variability of the background temperature field. The equatorial region below 85 km is dominated by the MSAO in temperature and zonal wind (Garcia and Clancy, 1990; Lieberman *et al.*, 1993). Because of *UARS* orbital precession, HRDI observations at 0600 and 1700 LT may be collected as far as a month apart. Thus, the 0600 and 1700 LT fields, as well as their difference, con-
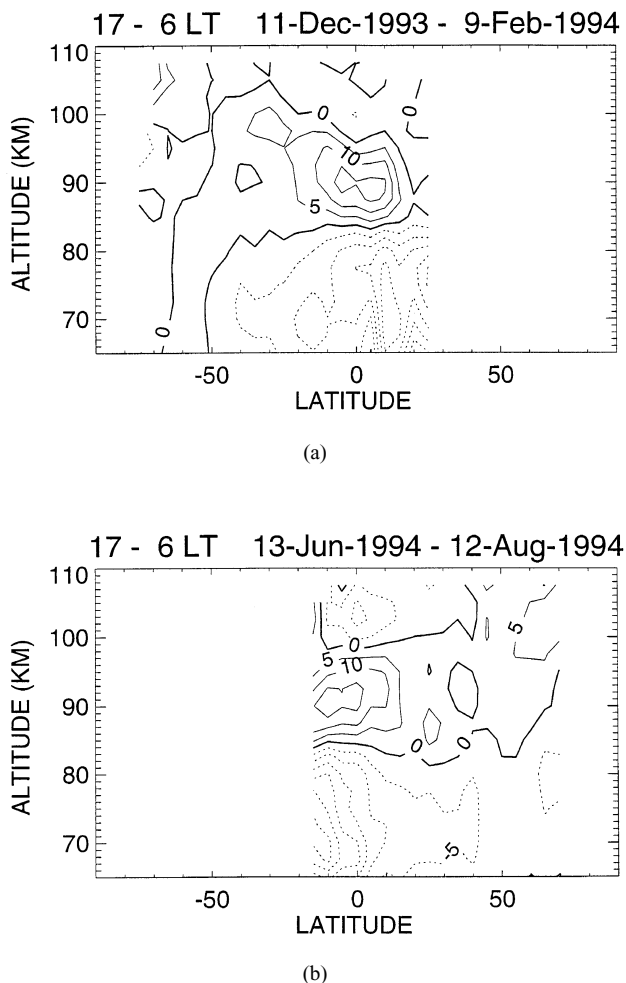
(a)

(b)

Fig. 9.   Difference between HRDI zonal mean temperatures at 1700 and 0600 LT, divided by two. (a) 11 December 1993–9 February 1994. (b) 13 June–12 August 1994.

tain variations in the background state along with the diurnal tide. Similar statements are true for the 11-hour difference in zonal winds (not shown).

Figures 8 and 9 clearly indicate that diurnal tides of significant amplitude are present in the daytime HRDI winds and temperature, which are not fully removed under 12-hour (i.e., 60-day) averaging. Thus, from the satellite perspective, the zonally averaged variables in Eqs. (1)–(10) represent the sum of the time-averaged zonal mean, and a diurnal tidal residue. The tidal presence in winds and temperatures suggests that when applied to HRDI data at low latitudes, (1) should be modified to include a tendency term reflecting aliasing by the diurnal tide. Equation (1) is then rewritten as

$$\frac{d\overline{V}}{dt} + \overline{U}\left(f + \frac{\overline{U}\tan\phi}{a}\right) = -\frac{\overline{\Phi}_\phi}{a} \qquad (11)$$

where $\overline{V}$ corresponds to the diurnal meridional wind. Assuming that the temporal variation of $\overline{V}$ is described by $V_0 \cos(\Omega(t' - t'_{max}))$ (here t' is local time), then the meridional diurnal tendency is of the form $-\Omega V_0 \sin(\Omega(t' - t'_{max}))$. If the diurnal tides are the primary source of the meridional momentum residual, then the imbalance between the Coriolis,

radial and pressure gradient forces (plotted in Fig. 7) is also well described by $-\Omega V_0 \sin(\Omega(t' - t'_{max}))$. Since (1,1) propagates downward in local time (Hays *et al.*, 1994), the low-latitude meridional momentum residues in Fig. 7 might be expected to resemble the product of Ω with the fields in Fig. 8 shifted upward by one-quarter cycle.

Comparison of Figs. 7 and 8 indicate that in the tropical winter latitudes, a southward acceleration maximum centered at 100 km is fairly well-correlated with a node in the diurnal meridional wind. The node is situated at an altitude where a southward tidal wind maximum occurs if the diurnal patterns in Fig. 8 are shifted upward by one quarter-cycle. Similar behavior of the opposite sign is observed on the other side of the equator. An additional region of northward acceleration centered at 85 km and 30°N is similarly correlated with tidal node structure and a northward maximum one quarter-cycle below. Assuming tidal amplitudes of about 25 m s^{-1}, this would correspond to a maximum tide-related acceleration of about ±160 m s^{-1}day^{-1}. This value is consistent with the acceleration in the tropical summer hemisphere during June–August 1994. However, in the winter hemisphere, and in both hemispheres during December–February, the observed accelerations near 100 km are at least a factor of two stronger. Thus, while aliasing by diurnal tides may account for a significant component of the low-latitude ageostrophy in Fig. 7, other factors may be contributing as well. Although diurnal tides clearly dominate the meridional winds, Fig. 8 suggests the presence of additional non-diurnal components, most notably at high latitudes. These could include a climatological mean meridional wind, as well as contamination from a semidiurnal tide with a time-varying amplitude. The momentum residuals in Fig. 7 might therefore be ascribed to diurnal and semidiurnal aliasing, advection of tidal and time-mean momentum by the mean meridional circulation, and gravity-wave, tidal and planetary-wave driving.

Finally, the effects of diurnal tides upon the terms in Eq. (10) are examined. Figure 10(a) shows a monthly mean composite of diurnal temperatures at the equator. This plot is analogous to Fig. 4(a), obtained by substituting HRDI daytime winds with diurnal temperatures evaluated at the local times sampled by HRDI. Diurnal temperature estimates used to create Fig. 10(a) are determined from HRDI diurnal meridional wind climatologies via classical tidal theory in the manner described by Lieberman and Hays (1994) and Lieberman (1997). Diurnal zonal winds and temperatures obtained in this manner at the equator are consistent with the more sophisticated, "tuned" diurnal estimates of Khattatov *et al.* (1997) and Yudin *et al.* (1997) (Lieberman, 1998). Diurnal equatorial temperatures peak near 95 km, and exhibit a prominent semiannual variation with the strongest amplitudes at equinox. The effects of the tidal oscillation are quite visible in the perturbation temperature field (Fig. 4(b)) above 90 km, where they account in part for the warm perturbations at equinox and the cold perturbations at solstice.

Figure 10(b) shows the RHS of Eq. (10) when it is applied to the diurnal temperature data, with the time-mean component removed. (The LHS, or vertical shear associated with the diurnal zonal wind at the equator, is an order of magnitude weaker and is not shown.) The large amplitudes of

COMPOSITE TEMP

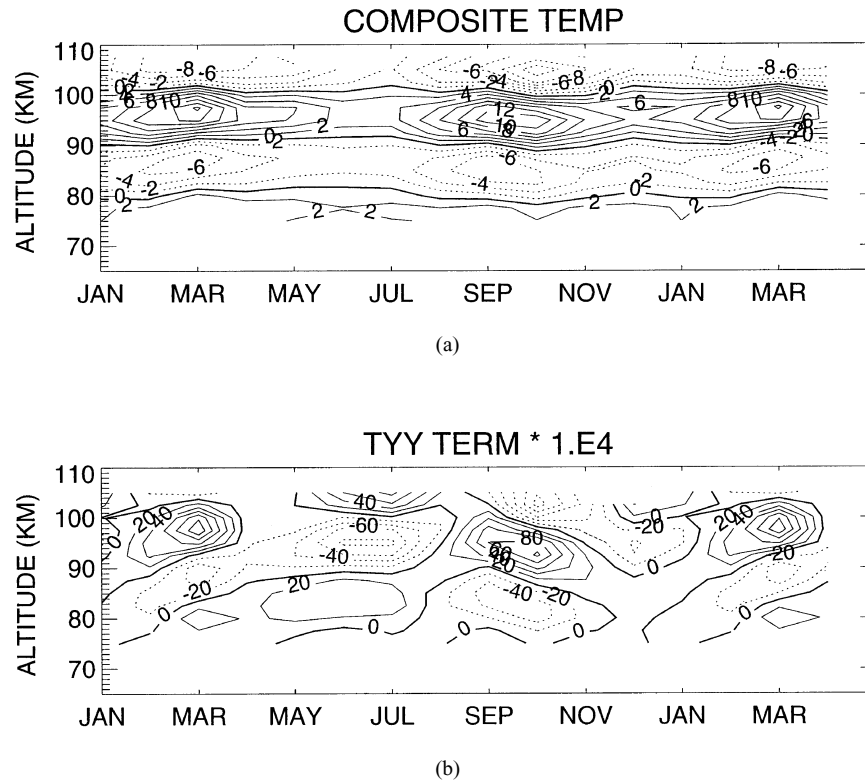(a)

TYY TERM * 1.E4

(b)

Fig. 10.   (a) As in Fig. 4(a), with HRDI wind values replaced with classical tidal estimates of diurnal temperature (see text). (b) As in Fig. 6(b), using diurnal temperatures with the time mean removed.

the diurnal tide correspond to strong meridional curvatures of the equatorial temperature. The tide-induced values of the RHS of (10) result in strong positive values at 95 km at equinoxes, and negative values at solstices. These patterns are well-correlated with the values corresponding to HRDI temperatures above 90 km (shown in Fig. 6(b)). Thus, the presence of tides in daytime temperatures are a likely source of the inconsistency between vertical wind shears derived from HRDI winds and from temperatures above 90 km.

5.   Summary

Gradient zonal mean winds computed from HRDI temperatures are compared with independently measured HRDI zonal mean winds. The gradient wind field contains the key observed features in the midlatitude summer hemisphere. These include the closure of the mesospheric easterly jet, the reversal to westerly flow above 90 km, and the closure of the westerly jet near 100 km. Consistency between gradient and observed HRDI winds deteriorates at tropical latitudes, where gradient winds exhibit excessive westerly shear. A geostrophic wind relation at the equator derived by applying L'Hopitals rule (1989) is examined. The vertical wind shear is qualitatively consistent with the curvature of the equatorial temperature field below 90 km. However, tidal contamination of daytime equatorial temperatures gives rise to very large differences between the RHS and LHS terms of (8) above 90 km.

Significant ageostrophy is present in the summer hemisphere at higher latitudes and altitudes. The meridional mo-

mentum residual in these regions may be indicative of drag due to meridionally propagating gravity waves, and momentum advection by the mean meridional circulation. Strong ageostrophic winds are also inferred at low latitudes. While these patterns may arise from wave drag and advective forces in the tropics, they are likely indicative of tidal aliasing. Because the propagating diurnal tides cannot be fully filtered from the daytime temperatures and winds, geostrophic balance cannot be realized in the HRDI data at low latitudes.

It is illuminating to consider the average of two global temperature fields observed nearly 12 hours apart. While the difference field in Fig. 9 highlights a fixed phase of the diurnal tide, the summed (or average) field is expected to emphasize the time-mean temperature field with diurnal effects minimized (although semidiurnal effects are retained). Figure 11 shows the average of HRDI temperatures sampled at 0600 and 1700 LT. Comparison of this field with Fig. 2 shows some subtle but important differences at low latitudes. During 11 December 1993–9 February 1994, the vertical structure of the 11-hour sum field between 20°S and 25°N is somewhat diminished. The area enclosed by the 200K contour between 80 and 90 km has shrunk, resulting in the disappearance of the temperature inversion between 5°S and 5°N, and poleward of 20°N. A warm region (between 180 and 190K) seen in Fig. 2 above the equator near 95 km has been almost eliminated in the 11-hour average field. These features suggest that incomplete removal of diurnal tides may account in part for the inversion layers observed below 90 km (Fig. 2). A similar finding was reported for
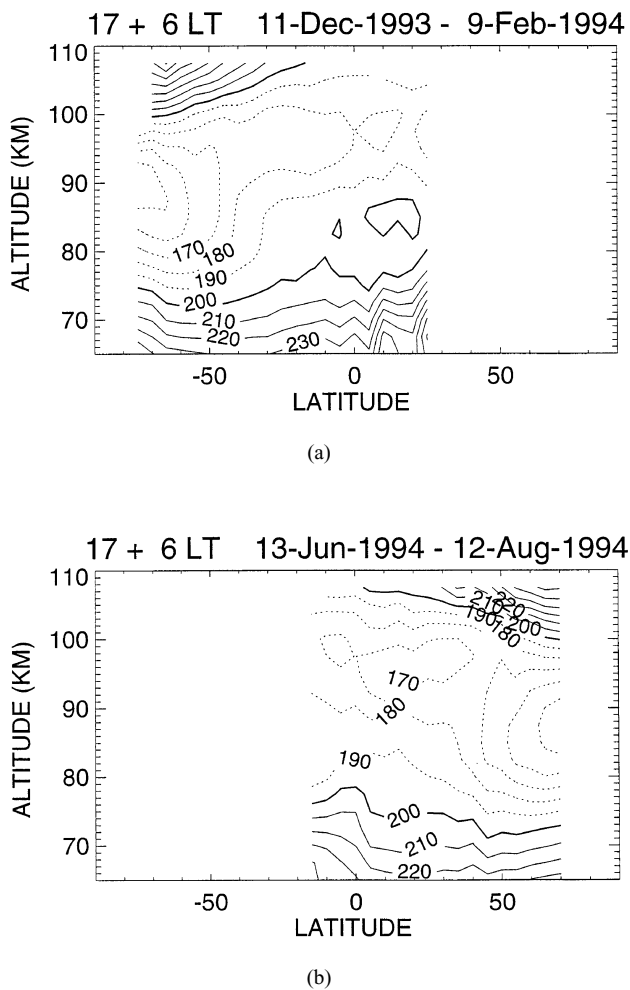
(a)

(b)

Fig. 11. Sum of HRDI 1700 and 0600 LT zonal mean temperature fields, divided by two (a) 11 December 1993–9 February 1994. (b) 13 June–12 August 1994.

lidar temperature climatologies at Urbana (40°, 88°W) derived from daytime and nighttime measurements (States and Gardner, 1998).

The contamination of HRDI daytime zonally averaged data by diurnal tides gives rise to strong horizontal and meridional gradients at low latitudes, thereby rendering the temperatures ineffectual for computing low-latitude balanced winds. Proper filtering of global-scale ageostrophic circulations such as tides is imperative in order to carry out an unambiguous, global assessment of MLT gradient wind balance. Hopefully, the emergence of daytime and nighttime resonance lidar measurements, and the anticipated day-night MLT coverage during the Thermosphere-Ionosphere-Mesosphere Energetics and Dynamics (TIMED) mission will enable this objective to be realized.

References

Abreu, V. J., A. Bucholtz, P. B. Hays, D. A. Ortland, W. R. Skinner, and J.-H. Yee, Absorption and emission line shapes in the O_2 atmospheric bands: Theoretical model and limb viewing simulations, *Appl. Opt.*, **28**, 2128–2137, 1989.

Andrews, D. G., J. R. Holton, and C. B. Leovy, *Middle Atmosphere Dynamics*, Academic Press, Orlando, FL, 1987.

Burrage, M. D., N. Arvin, W. R. Skinner, and P. B. Hays, Observations of the O_2 atmospheric band nightglow by the High Resolution Doppler Imager, *J. Geophys. Res.*, **99**, 15,017–15,023, 1994.

Burrage, M. D., M. E. Hagan, W. R. Skinner, D. L. Wu, and P. B. Hays, Long-term variability in the solar diurnal tide observed by HRDI and simulated by the GSWM, *Geophys. Res. Lett.*, **22**, 2641–2644, 1995.

Burrage, M. D., R. A. Vincent, H. G. Mayr, W. R. Skinner, N. F. Arnold, and P. B. Hays, Long term variability in the equatorial middle atmosphere zonal wind, *J. Geophys. Res.*, **101**, 12,847–12,854, 1996a.

Burrage, M. D., W. R. Skinner, D. A. Gell, P. B. Hays, A. R. Marshall, D. A. Ortland, A. H. Manson, S. J. Franke, D. C. Fritts, P. Hoffman, C. McLandress, R. Niciejewski, F. J. Schmidlin, G. G. Shepherd, W. Singer, T. Tsuda, and R. A. Vincent, Validation of mesospheric and lower thermospheric winds from the high resolution Doppler imager, *J. Geophys. Res.*, **101**, 10,365–10,392, 1996b.

Chapman, S. and R. S. Lindzen, *Atmospheric Tides*, Gordon and Breach, New York, 1970.

Fleming, E. R. and S. Chandra, Equatorial zonal wind in the middle atmosphere derived from geopotential height and temperature data, *J. Atmos. Sci.*, **46**, 860–866, 1989.

Fleming, E. R., S. Chandra, J. J. Barnett, and M. Corney, Zonal mean temperature, pressure, zonal wind and geopotential height as functions of latitude, *Adv. Space Res.*, **10**, 11–59, 1990.

Fleming, E. R., S. Chandra, M. D. Burrage, W. R. Skinner, P. B. Hays, B. H. Solheim, and G. G. Shepherd, Climatological mean wind observations from the UARS high-resolution Doppler imager and wind imaging interferometer: Comparison with current reference models, *J. Geophys. Res.*, **101**, 10,455–10,473, 1996.

Forbes, J. M., Atmospheric tides 1. model description and results for the solar diurnal component, *J. Geophys. Res.*, **87**, 5222–5240, 1982.

Forbes, J. M., M. Kilpatrick, D. Fritts, A. H. Manson, and R. A. Vincent, Zonal mean and tidal dynamics from space: An empirical examination of aliasing and sampling issues, *Ann. Geophys.*, **15**, 1158–1164, 1997.

Garcia, R. R. and R. T. Clancy, Seasonal variation in equatorial mesospheric temperatures observed by SME, *J. Atmos. Sci.*, **47**, 1666–1673, 1990.

Garcia, R. R., T. J. Dunkerton, R. S. Lieberman, and R. A. Vincent, Climatology of the semiannual oscillation of the tropical middle atmosphere, *J. Geophys. Res.*, **102**, 26,019–26,032, 1997.

Hays, P. B., V. J. Abreu, M. E. Dobbs, D. A. Gell, H. J. Grassl, and W. R. Skinner, The high-resolution Doppler imager on the upper atmosphere research satellite, *J. Geophys. Res.*, **96**, 10,713–10,723, 1993.

Hays, P. B., D. Wu, M. D. Burrage, D. A. Gell, H. J. Grassl, R. S. Lieberman, A. R. Marshall, Y. T. Morton, D. A. Ortland, and W. R. Skinner, Observations of the diurnal tide from space, *J. Atmos. Sci.*, **51**, 3077–3093, 1994.

Hedin, A. E., E. L. Fleming, A. H. Manson, F. J. Schmidlin, S. K. Avery, R. R. Clark, S. J. Franke, G. J. Fraser, T. Tsuda, F. Vial, and R. A. Vincent, Empirical wind model for the upper, middle and lower atmosphere, *J. Atmos. Sol.-Terr. Phys.*, **58**, 1421–1447, 1996.

Hitchman, M. H. and C. B. Leovy, Diurnal tide in the equatorial middle atmosphere as seen in LIMS temperatures, *J. Atmos. Sci.*, **42**, 557–561, 1985.

Hitchman, M. H. and C. B. Leovy, Evolution of the zonal mean state in the equatorial middle atmosphere during October 1978–May 1979, *J. Atmos. Sci.*, **43**, 3159–3176, 1986.

Huang, T. Y. W. and A. K. Smith, The mesospheric diabatic circulation and the parameterized thermal effect of gravity wave breaking on the circulation, *J. Atmos. Sci.*, **48**, 1093–1111, 1991.

Khattatov, B. V., M. A. Geller, V. A. Yudin, P. B. Hays, and R. A. Vincent, Diurnal migrating tide as seen by HRDI/UARS. part 1: Monthly mean global meridional winds, *J. Geophys. Res.*, **102**, 4405–4422, 1997.

Leblanc, T. and A. Hauchecorne, Recent observations of mesopause temperature inversions, *J. Geophys. Res.*, **102**, 19,471–19,482, 1997.

Leovy, C. B., Simple models of thermally driven mesospheric circulations, *J. Atmos. Sci.*, **21**, 327–341, 1964.

Lieberman, R. S., Nonmigrating diurnal tides in the equatorial middle atmosphere, *J. Atmos. Sci.*, **48**, 1112–1123, 1991.

Lieberman, R. S., Long-term variation of zonal mean winds and (1,1) driving

in the equatorial lower thermosphere, *J. Atmos. Sol.-Terr. Phys.*, **59**, 1483–1490, 1997.

Lieberman, R. S., Intraseasonal variability of HRDI winds in the equatorial mesosphere and lower thermosphere, *J. Geophys. Res.*, **103**, 11,221–11,228, 1998.

Lieberman, R. S. and P. B. Hays, An estimate of the momentum deposition in the lower thermosphere by the observed diurnal tide, *J. Atmos. Sci.*, **51**, 3094–3105, 1994.

Lieberman, R. S., M. D. Burrage, D. A. Gell, P. B. Hays, A. R. Marshall, D. A. Ortland, W. R. Skinner, and D. L. Wu, Zonal mean winds in the equatorial mesosphere and lower thermosphere observed by the High resolution Doppler Imager, *Geophys. Res. Lett.*, **20**, 2849–2852, 1993.

Manson, A. H., C. E. Meek, E. Fleming, S. Chandra, R. A. Vincent, A. Phillips, S. K. Avery, G. J. Fraser, M. J. Smith, J. L. Fellous, and M. Massebeuf, Comparisons between satellite-derived gradient winds and radar-derived winds from the CIRA-86, *J. Atmos. Sci.*, **48**, 411–428, 1991.

McLandress, C., G. G. Shepherd, and B. H. Solheim, Satellite observations of thermospheric tides: Results from the wind imaging interferometer on UARS, *J. Geophys. Res.*, **101**, 4093–4114, 1996.

Morton, Y. T., R. S. Lieberman, P. B. Hays, D. A. Ortland, A. R. Marshall, D. Wu, W. R. Skinner, M. D. Burrage, D. A. Gell, and J. H. Yee, Global mesospheric tidal winds observed by the High Resolution Doppler Imager on board the Upper Atmosphere Research Satellite, *Geophys. Res. Lett.*, **20**, 1263–1266, 1993.

Ortland, D. A., P. B. Hays, W. R. Skinner, M. D. Burrage, A. R. Marshall, and D. A. Gell, A sequential estimation technique for recovering atmospheric data from orbiting satellites, in *The Upper Mesosphere and Lower Thermosphere: A Review of Experiment and Theory*, volume 87 of *Geophysical Monograph series*, edited by R. Johnson and T. Killeen, pp. 329–337, American Geophysical Union, Washington, D.C., 1995.

Ortland, D. A., P. B. Hays, W. R. Skinner, and J. H. Yee, Remote sensing of mesospheric temperature and $O_2(^1\Sigma)$ band volume emission rates with the high resolution Doppler imager, *J. Geophys. Res.*, **103**, 1821–1835, 1998.

Palo, S. E. and S. K. Avery, Mean winds and the semiannual oscillation in the mesosphere and lower thermosphere at Christmas Island, *J. Geophys. Res.*, **98**, 20,385–20,400, 1993.

Randel, W. J., The evaluation of winds from geopotential height data in the stratosphere, *J. Atmos. Sci.*, **44**, 3097–3120, 1987.

Schoeberl, M. R., D. F. Strobel, and J. P. Apruzese, A numerical model of gravity wave breaking and stress in the mesosphere, *J. Geophys. Res.*, **88**, 5249–5259, 1983.

She, C. Y., J. R. Yu, D. A. Krueger, R. Roble, P. Keckhut, A. Hauchecorne, and M. L. Chanin, Vertical structure of the midlatitude temperature from stratosphere to mesosphere (30–105 km), *Geophys. Res. Lett.*, **22**, 377–380, 1995.

States, R. J. and C. S. Gardner, Influence of the diurnal tide and thermospheric heat sources on the formation of mesospheric temperature inversion layers, *Geophys. Res. Lett.*, **25**, 1998 (to appear).

Wallace, J. M. and F. R. Hartranft, Diurnal wind variations, surface to 30 kilometers, *Mon. Wea. Rev.*, **97**, 446–455, 1969.

Wallace, J. M. and R. F. Tadd, Some further results concerning the vertical structure of atmospheric tidal motions within the lowest 30 kilometers, *Mon. Wea. Rev.*, **102**, 795–803, 1974.

Yudin, V. A., B. V. Khattatov, M. A. Geller, D. A. Ortland, C. McLandress, and G. G. Shepherd, Thermal tides and studies to tune the mechanistic tidal model using UARS observations, *Ann. Geophys.*, **15**, 1205–1220, 1997.

R. S. Lieberman (e-mail: ruth@colorado-research.com)